J Solid State Electrochem (2005) 9: 146–153
DOI 10.1007/s10008-004-0567-0

ORIGINAL PAPER

Siyu Ye · Ashok K. Vijh

Oxygen reduction on an iron–carbonized aerogel nanocomposite electrocatalyst

Published online: 20 August 2004

Abstract Iron–carbonized aerogel nanocomposite was prepared from highly porous polyacrylonitrile microcellular foams containing a salt of iron, followed by carbonization. The electrochemical reduction of oxygen at this material was studied by using the rotating disk electrode method. In common with Pt/C, iron–carbonized aerogel nanocomposite presented excellent electrocatalytic activity for the oxygen reduction under experimental conditions close to those of a fuel cell cathode, that is, at the catalyst/Nafion interface in acidic solutions.

Keywords Non-noble metal catalyst · Oxygen reduction · Aerogel · Iron · Nanocomposite

Introduction

Electrocatalysis of the oxygen reduction reaction is of theoretical and practical interest because of its paramount importance in fuel cells and metal/air batteries [1, 2, 3], and in industrial electrolysis. Fuel cells, especially polymer electrolyte membrane fuel cells (PEMFCs), are attractive power sources for transportation, portable and stationary applications, due to their high efficiency, high power density and very low environmental impact [1, 2]. PEMFC is an electrochemical power generator that functions at low pH (PEM is constituted by a polymer electrolyte such as Nafion, which is a perfluoropolymer sulfonic acid with a gross equivalent concentration of about 0.1 M H^+ [4]). Until now only Pt and its alloys have been found suitable as catalysts for the hydrogen oxidation and oxygen reduction reactions in the commercial prototypes. Platinum is, however, a very expensive noble metal, and is also subject to a very limited supply. Thus, there has been an extensive activity in recent years to reduce the platinum loading while still meeting performance targets [5, 6], and, to develop electrocatalysts based on non-noble metals [7, 8, 9, 10, 11, 12]. However, the choice of non-noble metal-based materials which are suitable for this purpose is severely limited since the catalyst must not only have a high activity for the electrochemical reduction of oxygen (or oxidation of hydrogen), but must also be capable of withstanding the hostile environment of a fuel cell for a long period. The most challenging problem in the commercialization of PEMFC remains the search for highly efficient, stable and low-cost electrode materials. Non-noble metal-containing macrocycles such as phthlocyanines, porphyrins and their derivatives have been used as electrocatalysts for oxygen reduction for a long time, and seem to be one of the most promising potential materials to replace the expensive noble metal catalysts in PEMFCs [7, 9, 13, 14, 15, 16, 17, 18]. Previous work has also demonstrated that it is not necessary to use complex macrocycle precursors to obtain active catalysts for oxygen reduction by pyrolysis under high temperature conditions [8, 19, 20, 21, 22, 23, 24, 25]. These experiments appear to show that only a metal salt, a nitrogen donor and a carbon support are required to prepare active catalysts. This provides an attractive and a much cheaper way to prepare O_2 reduction catalysts. Although the source of the catalytic activity in these materials is not completely understood, the interaction between the transition metal and the nitrogen is believed to be an important factor.

Highly porous materials have recently been used extensively as substrates that provide nucleation sites for catalytic metal or metal oxide particles [26]. The porous nature of these materials minimizes the aggregation of the particles, and imposes an upper limit on their size. We have recently reported the use of highly porous

S. Ye (✉) · A. K. Vijh
Institut de Recherche d'Hydro-Québec,
1800 boul. Lionel-Boulet, Varennes, Québec,
J3X 1S1, Canada
E-mail: siyu.ye@ballard.com

Present address: S. Ye
Ballard Power Systems, 4343 North Fraser Way, Burnaby,
BC, V5J 5J9, Canada

carbonized aerogels as a novel support for fuel cell electrocatalysts [27, 28, 29, 30, 31, 32]. These new platinum–carbonized aerogel nanocomposites show excellent electrocatalytic activity for fuel cell reactions with a very low platinum loading. Our finding from the previous work on platinum–carbonized aerogel nanocomposites is that there exists a specific interaction between platinum and the nitrogen species of the carbonized aerogels and this observation led us to extend the work to non-noble metals. Very homogeneous Fe– or Co–carbonized aerogel nanocompostes were obtained, and were reported in a preliminary communication [33]. In the work reported in this paper, the electrochemical reduction of oxygen was studied at iron–carbonized aerogel nanocomposite by using the rotating disk electrode method. In common with Pt/C, iron–carbonized aerogel nanocomposite presented excellent electrocatalytic activity for the oxygen reduction under experimental conditions closed to those of a fuel cell cathode, that is, at the catalyst/Nafion interface in acidic solution.

Experimental

The non-noble metal–carbonized PAN aerogel composites were prepared according to a procedure similar to that described previously [27, 28, 29, 30, 31, 32, 33]. Briefly, an inorganic salt (e.g., $Fe(NO_3)_3$), in a ratio of 1 mmol per gram of PAN, was mixed with PAN (5 wt.%) in *N*,*N*-dimethylformamide (DMF)/water (v/v: 84/16). This mixture became a clear solution as the temperature increased. At about 120 °C, the solution was degassed and then poured into a mold. Upon cooling the solution, a polymer gel containing the metallic compound was obtained by thermally induced phase separation. The remaining solvent in the gel was exchanged with acetone or ethanol, and the latter solvent was removed by CO_2 supercritical extraction. The dry metal-containing PAN aerogel was pretreated in a forced-air convection oven at 220 °C, followed by pyrolysis at 900 °C under an argon atmosphere. The materials prepared by this method were denoted as PAN–Fe.

The electrode structure was fabricated as follows: the ground PAN–Fe powder was ultrasonically dispersed in a mixture of pure alcohol/water (v/v = 1/1) to produce a suspension of 7.5 mg/ml. A small amount of the suspension (typically 6 µl) was spread onto a glassy carbon electrode (diameter 4.0 mm, EG&G). After evaporation of the alcohol/water droplet, another 6 µl was spread on top of the coating, and this step was repeated again if higher PAN–Fe loading was needed. 6 µl of a 5 wt.% Nafion in alcohol–water solution (Aldrich) was put on top of the dried catalyst powder thereafter. The stability of the coatings was improved by a heat treatment at 75 °C for 5 min.

For comparison, 1% Pt/Vulcan XC72 fuel cell catalyst (E-TEK) was used to prepare an electrode structure by the same procedures described above, and was denoted as Pt/C.

All chemicals were of analytical grade purity and were used without further purification. Solutions were prepared using doubly distilled water. All experiments were performed at room temperature.

The rotating disk electrode experiments were conducted using a PAR Model 273 potentiostat/galvanostat coupled with Model 616 rotating disk electrode. A conventional H-type glass cell with a platinum foil or wire spiral counter-electrode was used for all electrochemical experiments. An Hg/Hg_2SO_4 electrode was used as the reference electrode; all potentials in this paper are referred to the normal hydrogen electrode (NHE). The sign of a cathodic current was defined as positive. Before each electrochemical experiment, ultra-pure Ar (Air Products) was passed through the 0.5-M H_2SO_4 aqueous solution for more than 30 min and cyclic voltammograms were obtained. Ultra-pure O_2 (Air Products) was then passed through the solution for more than 30 min and was kept bubbling through the solution during the oxygen reduction measurements. Cyclic voltammograms and polarization curves are given as current versus *E* plots, instead of current density versus *E*, due to the uncertainty of both the real and geometric surface area of the ink-type electrode [15].

Bulk concentration determinations were carried out by fusion gas technique on a Leco TC-136 System with a thermoconductivity detector (for oxygen/nitrogen) or a Leco CS-444 System with an IR detector (for carbon), or by Optima 4300 DV inductively coupled plasma optical emission spectrometers (ICP-OES, from Perkin-Elmer). The measurement precision is within ±2%.

Results and discussion

Composition

The composition of PAN–Fe is presented in Table 1. The iron content in this nanocomposite (10.4 wt%) is nearly double that in the initial feed (1 mmol per 1 g of PAN, that is, 5.3 wt%). The decomposition of PAN with the loss of some of the organic mass during carbonization is at the origin of the Fe enrichment of the final nanocomposite. It can also be seen from this table that the nitrogen content is very low, only 0.9 wt%, in comparison with 25 wt% in the initial feed. It is known from literature [34] that iron can catalyze the denitrification during carbonization of polyacrylonitrile. It may be the main reason that there is only 0.9 wt% of N remaining in this carbonized PAN–Fe nanocomposite.

Table 1 The bulk composition of PAN-Fe (in wt%)

C	N	O	Fe
84.4	0.9	4.0	10.4

Electrochemical behavior on a stationary electrode

The electrocatalytic property of PAN–Fe has been tested for the reduction of oxygen. Figure 1 shows the polarization curve of the PAN–Fe electrode in 0.5 M H_2SO_4 saturated with O_2, along with that in 0.5 M H_2SO_4 saturated with Ar. An enhancement of the cathodic current in the O_2-saturated solution indicates the electrocatalytic activity of the PAN–Fe for the reduction of oxygen. By contrast, the absence of large cathodic current in the oxygen reduction region is observed for the PAN aerogel without any metal [27]. It means that PAN aerogel without any metal was completely inactive for oxygen reduction in an acidic solution under the experimental conditions. Repeat cycling of the PAN–Fe in the O_2-saturated 0.5-M H_2SO_4 solution for more than 28 h did not show any change of the polarization curves. It indicates that the PAN–Fe material is promising as regards its stability under these experimental conditions.

Figure 2 shows the cyclic voltammograms of the PAN–Fe electrodes with different metal loading in 0.5 M H_2SO_4 saturated with O_2. These voltammograms were corrected for background currents by subtracting the voltammograms in an Ar atmosphere from those in an O_2 atmosphere. For comparison, the cyclic voltammogram of the Pt/C electrode with a Pt loading of 1.5 μg in 0.5 M H_2SO_4 saturated with O_2 is also shown in Fig. 2. It is possible to estimate the relative catalytic effect of materials by the cathodic peak potential at which the maximum oxygen reduction current occurs. A value closest to the theoretical reversible potential of 1.2 V for the oxygen reduction at room temperature indicates a superior catalytic activity. The peak potentials for PAN–Fe and Pt/C materials with different metal loadings are listed in Table 2. It is illustrated in Table 2 that O_2 reduction peak potential is, respectively, at about 0.6 V for PAN–Fe and 0.7 V for Pt/C, and it shifted positively a little with an increase of metal loading for both PAN–Fe and Pt/C. This means that the reaction overpotentials decrease and the catalytic activity increases with the metal loading within the range studied.

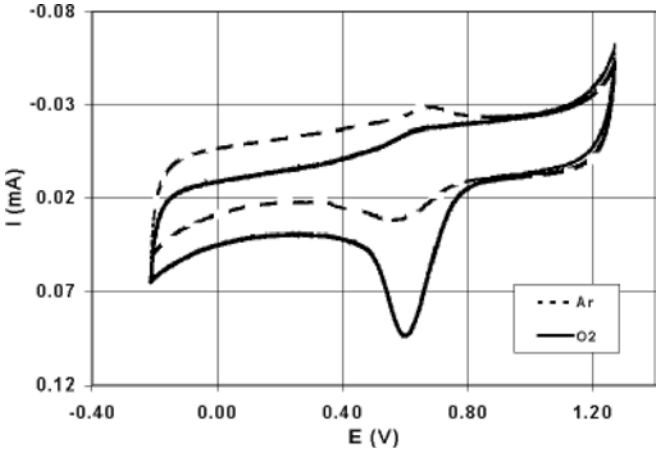

Fig. 1 Cyclic voltammograms of PAN–Fe with a Fe loading of 22.6 μg in 0.5 M H_2SO_4 saturated with Ar (- - -) and O_2 (—). Scan rate: 5 mV/s

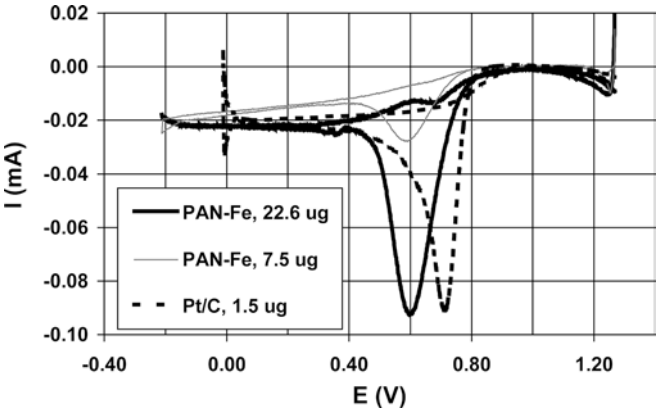

Fig. 2 Cyclic voltammograms of PAN–Fe with different Fe loadings in 0.5 M H_2SO_4 saturated with O_2. Cyclic voltammogram of Pt/C with a Pt loading of 1.5 μg is also shown here for comparison. Scan rate: 5 mV/s

Table 2 Oxygen reduction peak potentials (V versus NHE) of PAN-Fe and Pt/C with different metal loadings

Metal loading (μg)	PAN-Fe V (NHE)	Pt/C V (NHE)
0.75		0.70
1.5		0.71
7.5	0.58	
15	0.59	
22.6	0.60	

Kinetics at a rotating disk electrode

Since the oxygen reduction current depends strongly on hydrodynamic conditions, a rotating disk electrode was used to study the kinetics of oxygen reduction at PAN–Fe electrodes. Figure 3 presents the current-potential curves for PAN–Fe at rotation rate ω of 2,500 rpm (revolutions per minute) obtained by scanning the potential from 1.27 to −0.21 V at 5 mV s^{-1} in 0.5 M H_2SO_4 saturated with Ar (Fig. 3A) and O_2 (Fig. 3A). When the current–potential curve in an Ar atmosphere was subtracted from that in an oxygen atmosphere, the actual polarization curve for oxygen reduction was obtained (Fig. 3B). It can be seen that after correction for background current, there was no difference between polarization curves for oxygen reduction in the negative and positive sweep directions, except that there was a slight difference in the potential region 0.4–0.6 V. An ω-independent non-zero current value appeared at 0.8 V. Mass transport contributions became significant at lower potentials. In contrast to the curves for Pt/C (not shown here), the curves for PAN–Fe do not

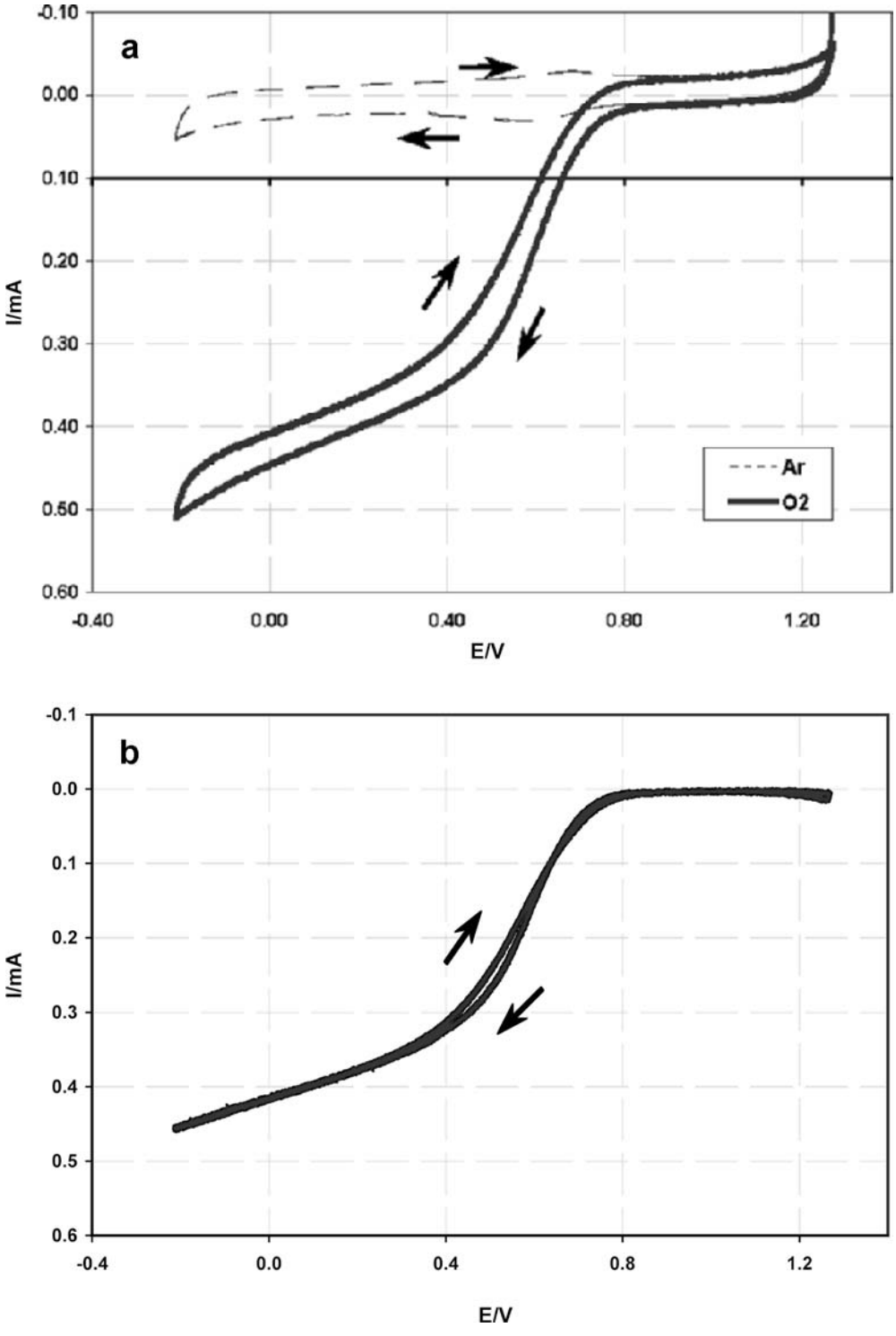

Fig. 3 Current–potential curves for PAN–Fe with a loading of 22.6 μg in 0.5 M H_2SO_4 saturated with Ar (**A**, - - -), O_2 (**A**, —) at 2,500 rpm. Scan rate: 5 mV/s. The curve after correction for the background current is shown in **B**

level off as expected at large overpotentials of O_2 reduction. There is no well-defined diffusion-limiting current plateau at any rotation rate. With increase of rotation rate, the plateau is more inclined. A similar shape of polarization curves was noted for O_2 reduction on ink-type of electrodes with a thin porous coating using different supported macrocycles [15, 35, 36]. It was considered to be an artifact of the porous coating electrode due to roughness or hydrodynamic flow in the porous coating caused by the pressure gradient across the face of the disk [15]. In porous electrodes, the depth of O_2 penetration inside the electrode structure changes with potential. If the electrocatalyst is Pt, O_2 reduction is fast enough that at high overpotentials the reaction is limited only on the outer part of the porous electrode, and a flat limiting plateau is observed

as for Pt/C [33]. For other electrocatalysts poorer than Pt, some of the electrocatalytic particles inside the electrode might be in contact with O_2 even at high overpotentials. Other explanations proposed considered a distribution of electrocatalytic sites on the electrode surface as responsible for such behavior. When distribution of active sites is less uniform and reaction is slower, the plateau is more inclined.

For a film-coated electrode, the overall measured current, I, is related to the kinetic current, I_k, the boundary-layer diffusion-limited current, I_L, and, film diffusion-limited current, I_f [37] by:

$$\frac{1}{I} = \frac{1}{I_k} + \frac{1}{I_L} + \frac{1}{I_f} \tag{1}$$

I_f represents the film diffusion-limited current controlled by reactant diffusion in the Nafion layer. It is defined as a function of the Nafion layer thickness, L, according to

$$I_f = \left(nFC_f D_f\right)L^{-1} \tag{2}$$

where D_f and C_f represent the diffusion coefficient and the solubility of the reactant in the Nafion layer, respectively.

I_L can be expressed as

$$I_L = 0.2nFc_{O_2}(D_{O_2})^{2/3}v^{-1/6}\omega^{1/2} \tag{3}$$

where c_{O_2} is the concentration of dissolved oxygen (1.1×10^{-6} mol cm^{-3}) [38], D_{O_2} its diffusion coefficient (1.4×10^{-5} cm^2 s^{-1}) [38], v the kinematic viscosity (0.01 cm^2 s^{-1} for sulfuric acid) [38], F the Faraday constant and n the apparent number of electrons transferred per molecule of O_2 in the overall reaction. The constant 0.2 is used when ω is expressed in revolutions per minute [39].

Eq. (1) can be simplified to

$$\frac{1}{I} = \frac{1}{I_k} + \frac{1}{I_f} + \frac{1}{B\omega^{1/2}} \tag{4}$$

where

$$B = 0.2nFc_{O_2}(D_{O_2})^{2/3}v^{-1/6} \tag{5}$$

Figure 4 shows the current–potential curves for PAN–Fe (with an iron loading of 22.6 μg cm^{-2}) at different rotation rates obtained by scanning the potential from 1.27 to −0.21 V at 5 mV s^{-1} in 0.5 M H_2SO_4 saturated with O_2. From the data of Fig. 4, the Koutecky–Levich plots (I^{-1}versus $\omega^{-1/2}$) were drawn (Fig. 5). At relatively high rotation speeds, a series of essentially parallel straight lines in the potential range of mixed kinetic–diffusion control regime is illustrated in Fig. 5, which indicates that the reaction order for the O_2 reduction at a PAN–Fe electrode is unity. Parallelism of the straight lines in Fig. 5 also indicates that the number of electrons transferred per O_2 molecule and active surface area for the reaction are not changed significantly within the potential range studied. The average slope values of those lines in Fig. 5 are 92 rpm$^{1/2}$ mA. If the geometric area of the glassy carbon substrate electrode (diameter 4 mm) was used, $n = 3.3$ was obtained by using Eq. (3) for PAN–Fe. However, it should be noted that due to the uncertainty of both the real and geometric surface area of the ink-type electrode, the number of electrons transferred per O_2 molecule, n, could not be calculated precisely. The more accurate determination of n as well as the percentage of peroxide released during the oxygen reduction reaction can be done by using rotating ring-disk electrode (RRDE) experiments where the knowledge of the mass transport limiting current is not required [18, 40, 41]; such studies could not be done, however, with the equipment and time available for this project in our laboratory.

A non-zero intercept of these lines in Fig. 5, even at very high overpotentials, where $1/I_k$ is negligible compared with the other terms in Eq. (4), demonstrates the effect of the reactant diffusion in the Nafion layer. Another effect that can contribute to the non-zero intercept may be due to the distribution of active sites, as

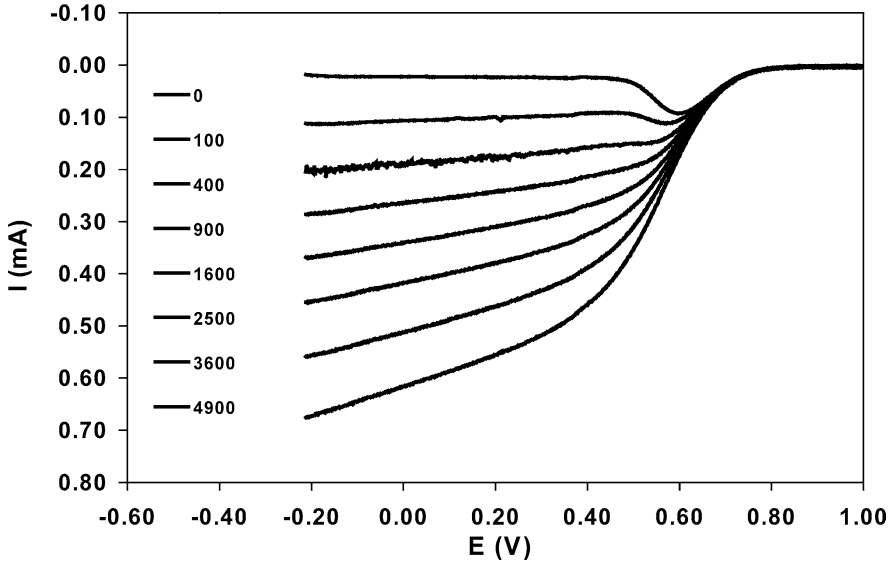

Fig. 4 Current–potential curves for PAN–Fe with a loading of 22.6 μg in 0.5 M H_2SO_4 saturated with O_2 at different rotation rates. Scan rate: 5 mV/s. The curves were background corrected

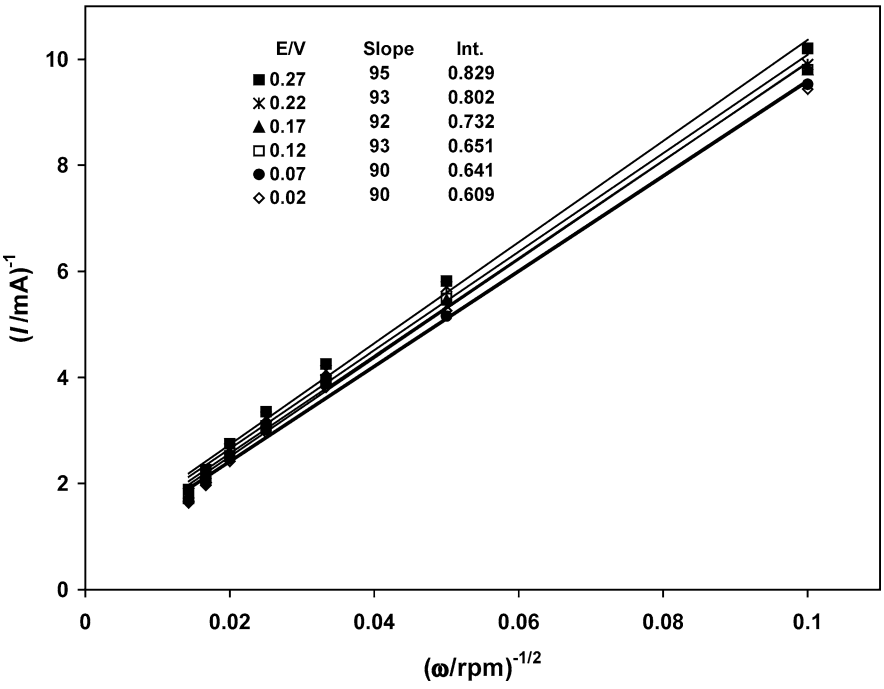

Fig. 5 Plots I^{-1} versus $\omega^{-1/2}$ for PAN–Fe at different potentials (shown in figures). These data were obtained from Fig. 4

discussed above, which makes it impossible to establish a complete diffusion control.

Tafel behavior

From Eqs. (3) and (4), the (net) kinetic current, I_K, can be derived:

$$I_K = \frac{I\, I_L}{I_L - I} \tag{6}$$

where $I_L/(I_L - I)$ is the mass transfer correction. Figure 6 shows the mass transfer-corrected Tafel plots (E versus log $II_L/[I_L - I]$) for O_2 reduction at the PAN–Fe electrode (with a metal loading of 22.6 μg) in 0.5 M H_2SO_4. Within the experimental error, this Tafel behavior is independent of ω that covers the range of rotation speeds from 400 to 4,900 rpm in the linear region of Fig. 6. Tafel slope of −57 mV decade^{-1} was obtained from the linear portion spanning about two decades of current density (Fig. 6). For heat-treated iron(III) tetramethoxyphenyl porphyrin chloride supported on

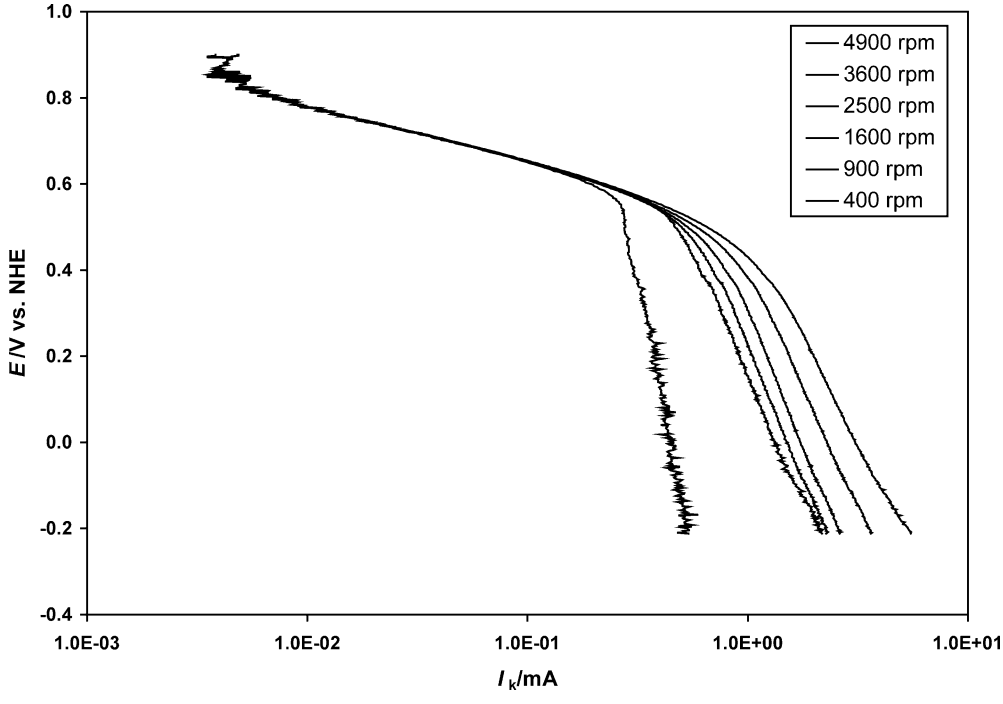

Fig. 6 Mass transfer-corrected Tafel plots for a PAN–Fe electrode in 0.5 M H_2SO_4 saturated with O_2. The rotation speeds are shown in the figure

Black Pearls carbon (FeTMMP-Cl/BP) as well as on Pt, a Tafel slope of -58 mV decade^{-1} was obtained, where this was ascribed to the transfer of the first electron as a rate-determining step and Temkin conditions of intermediate adsorption [36, 42]. At high currents, the slope changed with ω especially when ω is smaller than 400 rpm. The average of the Tafel slope values with ω higher than 400 rpm was -500 mV decade^{-1}. A similar Tafel slope for FeTMMP-Cl/BP has been obtained by Gojkvic et al. [36]. This value of the Tafel slope is anomalous in comparison with the results obtained from the rotating disk platinum electrode, which gave ≤ -120 mV decade^{-1} [38, 43]. This value could be caused by mass transfer limitation. The inner pore diffusion control has been invoked to account for the doubling of the Tafel slope [44]. Perry et al. [45], using their flooded-agglomerate, liquid-electrolyte model, also predicted a doubled Tafel slope when the oxygen reduction reaction is controlled by kinetics and ionic transport or the diffusion of dissolved O_2. In the case of kinetic, diffusion and ionic transport control, this model predicts a quadrupled Tafel slope. The Tafel slope estimated in the present work is approximately the quadruple of -120 mV decade^{-1} that can be expected for oxygen reduction at high current [38, 43].

We also previously described the anomalous Tafel slope using a very simple quantitative description [28] with the following equation:

$$i = \text{constant} \times \exp\left[-\frac{\beta(E - E_f)nF}{RT}\right] \tag{7}$$

where E is the total applied potential, and E_f the fraction of E that may operate across the inner pores.

In general, it might be assumed that E_f would be some fraction of E, thus:

$$\log i = \text{constant} - \frac{\beta(E - E_f)nF}{2.3RT} \tag{8}$$

On rearrangement and differentiation of Eq. (8), the Tafel slope is obtained as:

$$\frac{\partial E}{\partial \log i} = -\frac{2.3RT}{\beta nF(1 - \partial E_f/\partial E)} \tag{9}$$

In the absence of inner pores and with the usual values of β ($=0.5$) and n ($=1$), the Tafel slope would be -120 mV decade^{-1} at room temperature, as expected from theory. However, if 76% of the total applied potential operates across the inner pores, i.e., if $E_f = 0.76E$, the value of the Tafel slope from Eq. (9) would be -500 mV decade^{-1} at room temperature, which is what is obtained from Fig. 6. It should be mentioned that the argument contained in Eqs. (7) to (9) here was originally proposed in the context in which E_f represented the potential drop across a surface oxide film [46, 47].

It should also be noted that the dependence of currents on the rotation rate of the electrode may not allow us to correctly characterize the polarization curves at $E < 0.6$ V as Tafel plots. The ill-defined limiting current plateau is also a possible reason for the uncommon "Tafel behavior" at high currents.

Conclusions

Iron–carbonized aerogel nanocomposite was prepared for use as a fuel cell catalyst. This non-noble metal-based material presents unexpectedly high electrocatalytic activity for the oxygen reduction in acidic solutions. The cathodic peak potential at which the maximum oxygen reduction current occurs is 0.60 V for PAN–Fe, whereas for 1% Pt/C it is at 0.71 V. For PAN–Fe, the O_2 reduction potential shifted positively a little with the increase of metal loading, the same as for 1% Pt/C. From the RDE experiments, the number of electrons transferred per O_2 molecule, n, was determined to be 3.3. A Tafel slope of -57 mV decade^{-1} was obtained from the linear portion spanning about two decades of current density at low currents. An anomalous "Tafel slope" of -500 mV decade^{-1} was obtained at high currents.

Acknowledgements Thanks are due to Dr. Guy Bélanger of IREQ for his interest in this work.

References

1. Prater KB (1996) J Power Sources 61:105
2. Gottesfeld S, Zawodzinski TA (1997) Polymer electrolyte fuel cells. In: Alkire RC, Gerischer H, Kolb DM, Tobias CW (eds) Advances in electrochemical science and engineering, vol. 5. Viley-VCH, Weinheim, p 197
3. Larminie J, Dicks A (2000) Fuel cell systems explained, Wiley, Chichester
4. Appleby AJ (1993) J Electroanal Chem 357:117
5. Steele BCH, Heinzel A (2001) Nature 414:345
6. Wang X, Hsing I-M (2002) Electrochim Acta 47:2981
7. Adzic RR, Anson FC, Kinoshita K (eds) (1996) Proceedings of the symposium on oxygen electrochemistry. The Electrochemical Society, Pennington, NJ
8. Faubert G, Coté R, Guay D, Dodelet JP, Dénés G, Poleunis C, Bertrand P (1998) Electrochim Acta 43:1969
9. Jiang R, Chu D (2000) J Electrochem Soc 147:4605
10. Finkelshtain G, Katzman Y, Khidekel M, Borover G (2001) PCT Patent WO 01/15253 A1
11. Burstein GT, McIntyre DR, Vossen A (2002) Electrochem Solid-State Lett 5:A80
12. Jiang J, Kucernak A (2002) Electrochim Acta 47:1967
13. Steiger B, Shi S, Anson FC (1993) Inorg Chem 32:2107
14. Dignard-Bailey L, Trudeau ML, Joly A, Schulz R, Lalande G, Guay D, Dodelet JP (1994) J Mater Res 9:3203
15. Gojkovic SLj, Gupta S, Savinell RF (1998) J Electrochem Soc 145:3493
16. Okado T, Yoshida M, Hirose T, Kasuga K, Yu T, Yuasa M, Sekine I (2000) Electrochim Acta 46:4419
17. Sun GQ, Wang JT, Gupta S, Savinell RF (2001) J Appl Electrochem 31:1025
18. Lefèvre M, Dodelet JP (2003) Electrochim Acta 48:2749
19. Gupta S, Tryk D, Bae I, Aldred W, Yeager E (1989) J Appl Electrochem 19:19
20. Ohms D, Herzog S, Franke R, Neumann V, Wiesener K, Gamburcev S, Kaisheva A, Iliev I (1992) J Power Sources 38:327

21. Martin Alves MC, Tourillon G (1996) J Phys Chem 100:7566
22. He P, Lefèvre M, Faubert G, Dodelet JP (1999) J New Mater Electrochem Syst 2:243
23. Wang H, Coté R, Faubert G, Guay D, Dodelet JP (1999) J Phys Chem 103:2042
24. Bouwkamp-Wijnoltz AI, Visscher W, van Veen JAR, Tang SC (1999) Electrochim Acta 45:379
25. Wei G, Wainright JS, Savinell RF (2000) J New Mater Electrochem Syst 3:121
26. Ziolo RF, Giannelis EP, Weinstein BA, O'Horo MP, Ganguly BN, Mehrotra V, Russel MW, Huffman DR (1992) Science 257:219
27. Ye S, Vijh AK, Dao LH (1996) J Electrochem Soc 143:L7
28. Ye S, Vijh AK, Dao LH (1996) J Electroanal Chem 415:115
29. Ye S, Vijh AK, Dao LH (1997) J Electrochem Soc 144:90
30. Ye S, Vijh AK, Dao LH (1997) J Electrochem Soc 144:1734
31. Ye S, Vijh AK, Wang ZY, Dao LH (1997) Can J Chem 75:1666
32. Ye S, Vijh AK, Dao LH (1998) J New Mater Electrochem Syst 1:17
33. Ye S, Vijh AK (2003) Electrochem Commun 5:272
34. Zhu Z, Liu Z, Gu Y (1997) Fuel 76:155
35. Lalande G, Coté R, Guay D, Dodelet JP, Weng LT, Bertrand P (1997) Electrochim Acta 42:1379
36. Gojkovic SLj, Gupta S, Savinell RF (1999) J Electroanal Chem 462:63
37. Lawson DR, Whiteley LD, Martin CR, Szentimay MN, Song JI (1988) J Electrochem Soc 135:2247
38. Hsueh KL, Chin DT, Srinivasan S (1983) J Electroanal Chem 153:79
39. Zagal J, Bindra P, Yeager E (1980) J Electrochem Soc 127:1506
40. Claude E, Adou T, Latour JM, Aldebert P (1998) J Appl Electrochem 28:57
41. S.Lj. Gojkovic, S. Gupta, and R.F. Savinell (1999) Electrochim Acta 45:889
42. Šepa DB, Vojnović MV, Damjanović A (1981) Electrochim Acta, 26:781
43. Zinola CF, Castro Luna AM, Triaca WE, Arvia AJ (1994) J Appl Electrochem 24:119
44. Arico AS, Antonucci V, Alderucci V, Modica E, Giordano N (1993) J Appl Electrochem 23:1107
45. Perry ML, Newmann J, Cairns EJ (1998) J Electrochem Soc 145:5
46. Vijh AK (1973) Electrochemistry of metals and semiconductors, Marcel Dekker, New York, Chapter 6
47. Vijh AK (1969) J Phys Chem 73:506